Trees (2026) 40:14
https://doi.org/10.1007/s00468-025-02721-y

ORIGINAL ARTICLE

Tracking drought-driven hydraulic impairment in *Pinus sylvestris* with microtensiometry and dendrometry

Antonio M. Cachinero-Vivar[1,2] · Óscar Pérez-Priego[1,2]

Received: 31 October 2025 / Accepted: 29 December 2025

Abstract

Key message **Continuous monitoring of stem water potential and circumference variation reveals a relationship between apparent stem capacitance and Ψ-mapped embolism risk during drought, providing a mechanistic and practical proxy to assess hydraulic safety in mature conifers.**

Abstract Projected increases in drought frequency and intensity threaten the hydraulic function and survival of mature conifers. However, continuous in-situ monitoring of stem water status remains technically challenging, particularly within forest canopies. We deployed microtensiometers and precision dendrometers in a thinned *Pinus sylvestris* stand (Sierra Nevada, Spain) to monitor hourly stem water potential (Ψ_{STEM}) and stem circumference variation (*SCV*). Stem hydraulic capacitance (C_S) was derived in situ from SCV– Ψ_{STEM} time series. Embolism risk, *PLC (Ψ)*, was estimated at diagnostic intervals by mapping in-situ Ψ_{STEM} onto laboratory vulnerability curves. Continuous Ψ_{STEM} closely matched independent leaf pressure-chamber measurements ($R^2 = 0.78$) and covaried with sub-daily *SCV* dynamics, validating both sensors. Midday *SCV* (SCV_{MD}) covaried with midday Ψ_{MD} ($R^2 = 0.49$) and with Ψ-mapped embolism risk ($PLC\,(\Psi_{MD})$) ($R^2 = 0.51$), indicating that greater shrinkage aligns with more negative tension and higher estimated risk. Across the dry-down, *PLC* (*Ψ*) indicated rising risk while C_S declined; we interpret this as a plausible capacitance–risk linkage given our design. Concurrent eddy-covariance measurements showed late-summer attenuation of canopy latent energy (*LE*), with lower midday peaks and reduced diurnal amplitude-coincident with higher *PLC* (*Ψ*) estimates and declining C_S. Mixed-effects modeling revealed that *SCV* was jointly driven by Ψ_{STEM}, air temperature, vapor-pressure deficit, relative humidity, and most prominently soil water content. Together, these results demonstrate that non-destructive, high-temporal-resolution sensing resolves diel–seasonal hydraulics and support a capacitance–embolism risk trade-off. We further show that SCV_{MD} provides a practical proxy for hydraulic status where direct tensiometry is impractical, informing physiologically based forest management.

Antonio M. Cachinero-Vivar and Óscar Pérez-Priego have contributed equally to this work.

Communicated by Liang

✉ Antonio M. Cachinero-Vivar
o02cavia@uco.es

✉ Óscar Pérez-Priego
g72pepro@uco.es

[1] Department of Forest Engineering, Laboratory of Dasometry and Forest Management, University of Córdoba, Edif. Leonardo da Vinci, Campus de Rabanales s/n, Córdoba 14071, Spain

[2] Andalusian Institute of Earth System Research IISTA-CEAMA, Granada 18006, Spain

Published online: 20 January 2026

Graphical abstract

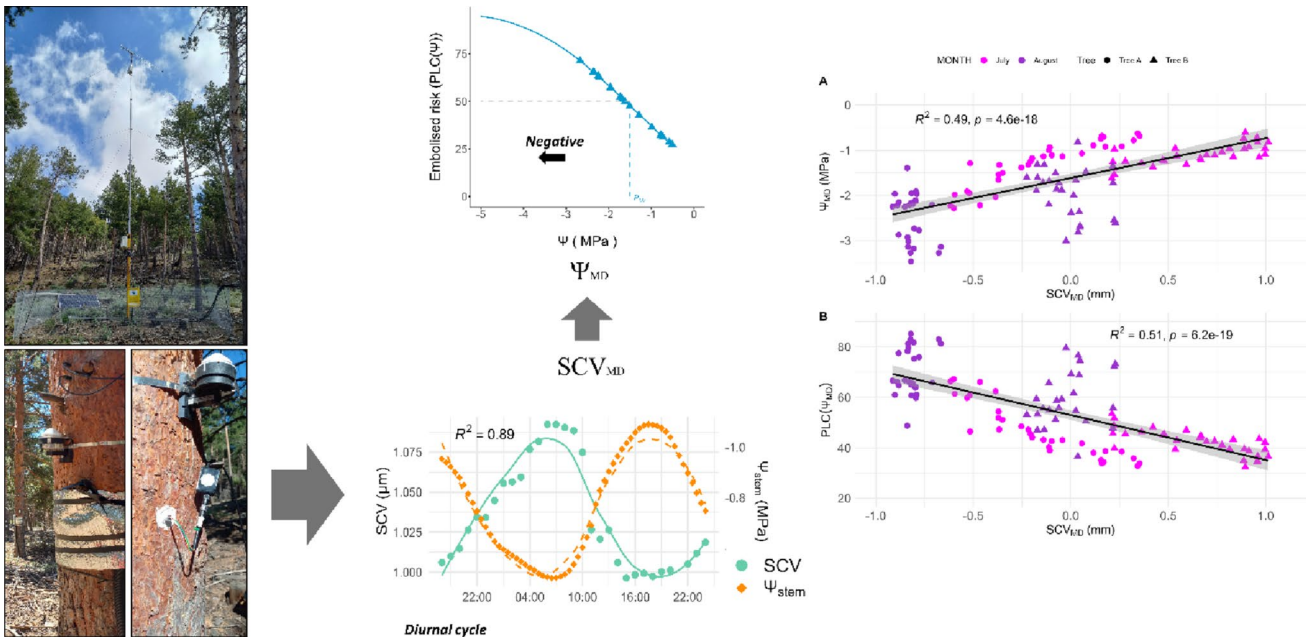

Keywords Microtensiometer · Digital dendrometers · Plant hydraulics · Vulnerability curves · Silviculture · Pinus spp.

Introduction

Projected increases in drought frequency and intensity across temperate forests pose a critical threat to conifer species, with implications for both ecosystem function and global carbon budgets (Allen et al. 2010; Spinoni et al. 2018). Tree mortality events linked to hydraulic failure are becoming increasingly common, especially among tall, mature individuals with high water demand and limited access to deep soil moisture. Drought responses in conifers are strongly species-specific, driven by differences in stomatal regulation, xylem vulnerability, and internal water storage (Senf et al. 2020; Schmied et al. 2022). However, empirical characterization of these hydraulic traits in mature forest trees remains challenging due to methodological constraints.

Water transport in conifers operates along gradients of water potential (Ψ) from soil to the atmosphere, maintained by transpiration-driven tension in the xylem (Thomas 1997). The efficiency and resilience of this continuum is modulated by key hydraulic traits such as stem hydraulic conductivity (K_S) and capacitance (Cs) (Choat et al. 2018). The former determines the rate at which water moves through xylem conduits, whereas Cs reflects the capacity of elastic tissues to store and release water, buffering short-term fluctuations in Ψ (Meinzer et al. 2003; Scholz et al. 2011; Wang and Zhang 2023). In dry environments, high Cs mitigates diurnal declines in Ψ by supplying water to the transpiration stream, delaying the onset of cavitation and preserving stomatal conductance (Brodribb and Cochard 2009; Arend et al. 2021). Conversely, reduced K_S due to embolism formation limits water transport and gas exchange, constraining carbon assimilation. Accurate measurements of Ψ are therefore essential to quantify both K_S and Cs, as they define the pressure–volume relationships that govern xylem function and water storage dynamics (Chhajed et al. 2024). The coordination between these traits ultimately determines the balance between hydraulic efficiency and safety, shaping plant performance and survival under drought.

Continuous in situ monitoring of hydraulic traits remains technically challenging due to limitations of conventional instrumentation. Traditional approaches—such as the Scholander pressure chamber for discrete water potential (Ψ) measurements and hydraulic flow meters for K_S determination—are labour-intensive, destructive, and provide only snapshot information under variable environmental conditions (Scholander et al. 1965; Novick et al. 2022; Haberstroh et al. 2022). Similarly, laboratory-based estimates of C_S derived from pressure–volume or dehydration curves capture static tissue properties rather than dynamic responses to fluctuating water status (Chhajed et al. 2024). Recent advances in microtensiometry and high-resolution dendrometry overcome many of these constraints by enabling continuous, non-destructive measurement of Ψ (Blanco and Kalcsits 2021; Haberstroh et al. 2025), and stem circumference variation (SCV; (Dietrich et al. 2018;

Ziegler et al. 2024) directly in the field. These tools allow real-time tracking of diurnal water potential dynamics and elastic tissue responses, offering unprecedented temporal resolution to quantify in situ hydraulic capacitance and infer conductivity changes during drought progression. Such continuous monitoring provides a powerful framework to link short-term hydraulic behaviour with long-term physiological performance in forest trees.

Maximum daily shrinkage (*MDS*)—the difference between predawn maximum and midday minimum stem radius—indexes elastic water release sustaining daytime transpiration. *MDS* typically rises early in drought and declines under advanced drought when dehydration and incomplete nocturnal refilling limit reversible shrinkage (Peters et al. 2025). Coupling *MDS* with continuous stem water potential (Ψ_{STEM}) from microtensiometers enables in-situ estimation of apparent stem hydraulic capacitance ($Cs \approx \Delta SCV/\Delta\Psi_{STEM}$) and helps separate hydraulic from purely atmospheric drivers. Where needed, laboratory vulnerability curves provide a Ψ-based diagnostic of embolism risk at defined intervals (e.g., Ψ_{50}, often P_{50}, as the xylem water potential at which 50% of maximum hydraulic conductivity is lost), without implying continuous *PLC* retrieval (Choat et al. 2008; Brodribb and Cochard 2009; Knüver et al. 2025).

Stem capacitance (C_S) and percent loss of conductivity (*PLC*) are functionally linked through their common dependence on water potential (Ψ): higher *Cs* buffers short-term declines in Ψ, delaying crossings of vulnerability thresholds (e.g., P_{50}) and thereby lowering instantaneous *PLC* (Ψ) risk (Meinzer et al. 2003; Brodribb and Cochard 2009; Choat et al. 2018). As embolism advances and conductive pathways become hydraulically disconnected, the volume of active storage effectively decreases, so apparent *Cs* can decline even though elastic tissues themselves do not reduce sapwood conductivity; loss of transport arises from embolism (and, under extreme tension, conduit collapse) rather than from elasticity per se (Tyree and Zimmermann 2002; Hölttä et al. 2009; Meinzer et al. 2009). This balance varies among species: isohydric trees rely on greater C_S to stabilize Ψ, whereas anisohydric species tolerate lower Ψ at the expense of higher *PLC* (Martínez-Vilalta et al. 2014; Anderegg et al. 2016; Bourbia et al. 2025). Combining *SCV*-derived C_S estimates with *PLC* measurements links dynamic water storage to hydraulic vulnerability in situ, offering insights into species-specific drought resilience and mortality risk while accounting for anatomical influences such as bark thickness and tissue elasticity.

Although microtensiometers have been successfully deployed in orchard and broadleaf species (Haberstroh et al. 2025), their integration with dendrometric monitoring in conifers—particularly pines— remains untested. Conifers possess distinctive hydraulic architectures and diverse drought-response strategies, yet the relationship between *Cs* and embolism risk inferred from vulnerability curves has not been well quantified. To address this knowledge gap, we employed an integrative in situ sensor framework in a thinned *Pinus sylvestris* stand with the following objectives:

i. Evaluate the performance of microtensiometer by comparing continuous stem water potential (Ψ_{STEM}) measurements with discrete predawn and midday leaf water potential (Ψ_{LEAF}) from a single diurnal cycle, and test correspondence with daily stem circumference variation (*SCV*) during daytime shrinkage and night-time rehydration.
ii. Test SCV_{MD} as a proxy for midday Ψ_{STEM} (Ψ_{MD}) during peak drought stress, providing a practical, non-destructive indicator where tensiometry is impractical.
iii. Quantify seasonal dynamics of stem hydraulic capacitance (*Cs*) and diagnose embolism risk at defined intervals by mapping in-situ Ψ_{STEM} onto laboratory vulnerability curves (*PLC* (Ψ)).

In this study, we combined continuous stem-circumference monitoring with direct assessments of stem water potential and hydraulic traits to examine drought-induced changes in stem water relations. Rather than retrieving a continuous *PLC* time series, we diagnosed embolism risk at defined intervals by mapping in-situ Ψ_{STEM} onto laboratory vulnerability curves (*PLC* (Ψ)), while deriving stem hydraulic capacitance (*Cs*) in situ from *SCV*–Ψ_{STEM}. Together, these diagnostics characterize how rising tension-based risk and declining internal buffering co-evolve through dry-down, advancing a physiologically grounded picture of conifer drought vulnerability under climate stress.

Materials and methods

Study area and tree specie

The study was conducted in the Sierra Nevada National Park, a mountainous region in southern Spain with elevations ranging from 860 to 3,482 m a.s.l. The area has a Mediterranean climate, marked by cold winters, hot summers, and an average annual precipitation of ~600 mm, with a pronounced dry season from mid-June to mid-September. Mean annual temperatures range from 12 to 16 °C at lower elevations to below 10 °C above 3,000 m. Natural forests cover approximately 20% of the park, while introduced pine species -*Pinus halepensis*, *P. pinaster*, *P. nigra*, and *P. sylvestris*-planted between 1960 and 1980, now occupy about 80% of the forested area. Field measurements were

performed in a *Pinus sylvestris* stand situated on the windward slope of the Mairena region, Sierra Nevada (37.04° N, 3.05° W; ~2,100 m a.s.l.). In 2018, a heavy thinning treatment was applied, reducing the stand's basal area by 70%. Within a representative 200 × 200 m plot, we selected 15 dominant trees for monitoring. The monitored trees had an average diameter at breast height (*DBH*) of 25.36 ± 0.81 cm and mean height of 11.17 ± 0.19 m. Stand density (*N*) and basal area (*G*) were 348 trees ha^{-1} and 17.57 m^2 ha^{-1}, respectively.

Stem dendrometer

In March 2023 five high-precision, band-type digital dendrometers (DRL-26 C, EMS Brno, CZ) were installed. Sensors were mounted at breast height (1.3 m) on trees using stainless-steel bands pre-tensioned to the manufacturer's specification. For the present analysis, we focused on two trees equipped with two dendrometers and four microtensiometers, monitored across one growing season. The monitored trees were located within approximately 10 m of elevation difference across the plot, experiencing similar microclimatic conditions. The devices logged stem-circumference variation (*SCV*) every 60 min with a resolution of ± 1 µm and an intrinsic thermal drift < 2 µm $°C^{-1}$. This level of thermal sensitivity is negligible compared with the diurnal amplitude of stem fluctuations, and the pre-tensioned stainless-steel band minimizes any mechanical slack or temperature-induced expansion. Consequently, non-hydraulic effects such as thermal expansion or band deformation were considered insignificant. *SCV* represents the relative change in stem circumference over time and was reset to 0 µm at the start of the Ψ_{STEM} measurements for each tree, when the probes were installed and the data became stable and reliable for correlation, starting at the end of June.

Raw *SCV* series were processed with the treenetproc R package (Haeni et al. 2020; Knüsel et al. 2021) for initial error correction and data formatting. The package was also used to derive maximum daily shrinkage (*MDS*) and maximum daily expansion (*MDE*) from the processed *SCV* series, capturing the reversible, water-related component of daily stem variation. Following Peters et al. (2025), *MDS* was normalized by the tree-specific maximum daily value (MDS_{max}), yielding $MDS_n = MDS / MDS_{max}$, which reduces inter-tree variability and enhances comparability across individuals and seasons (Fig. S4). In this study, MDS_{max} was determined over the 2023 growing season for the two analysed trees. For maximum comparability, multi-year baselines (≥ 3 years) are recommended (Peters et al. 2025). Normalised MDS_n is interpreted relative to this single-year maximum. MDS_n can be interpreted as a proxy for relative stem water capacitance, largely independent of growth and bark elasticity, and provides a dendrometer-derived indicator of drought stress intensity when interpreted alongside concurrent measures of transpiration.

Stem microtensiometer

In May 2024, four stem water potential sensors (two per tree; microtensiometers with piezoresistive pressure transducers; FloraPulse, CA, USA) were installed, following the manufacturer's recommendation to install sensors in pairs per tree. measuring 5 × 5 mm and housed in an 8 mm diameter cylindrical probe, were installed in two dominant *Pinus sylvestris* trees within the same thinned stand at approximately 2,100 m a.s.l. The trees were located about 2 m apart in elevation and experienced identical microclimatic conditions, serving as biological replicates within the same environmental setting. Installation followed the manufacturers protocol (Lakso et al. 2022; Pagay 2022): a provided sleeve (14 mm outer diameter, 9 mm inner diameter) was inserted into the stem, ensuring contact with active xylem tissue. Stem material within the sleeve was carefully drilled and removed to a depth of approximately 4–5 cm. All insertion sites displayed a bright white coloration, indicative of functional xylem. The sleeve was immediately filled with a fine clay paste, and the sensor probe was carefully inserted and secured. To prevent moisture ingress, the installation area was sealed with silicone grease (see Graphical abstract). Sensors were mounted at 1.3 m above the ground and shielded with reflective aluminium foil to minimize thermal interference from solar radiation. No additional maintenance was necessary until the scheduled inspection for re-operation, programmed 1.5 years after installation. Stem water potential (Ψ_{STEM}) was recorded every 30 min using a Campbell CR1000X data logger (Campbell Scientific, UT, USA). Installation-related disturbances caused readings to be inconsistent for 3–4 days, after which they stabilized and produced robust outputs.

Conventional leaf water potential measurements (Predawn Ψ_{LPD}, and midday $\Psi_{LMD;}$ MPa) were collected with a Scholander pressure pump (SKPM 1400, Skye Instruments, UK) on sunlit, uncovered branches of the two trees equipped with microtensiometers. Predawn and midday stem water potential (Ψ) were measured on a single day to capture diurnal dynamics and validate the Ψ_{STEM} microtensiometers. Predawn measurements were conducted just before sunrise (typically between 4:00 and 6:00 a.m.), and midday measurements around 12:00 to 2:00 p.m., coinciding with peak daily transpiration. Measurements were performed without delay after excision and insertion into the Scholander chamber, ensuring minimal Ψ changes due to handling. Continuous microtensiometer measurements were recorded from

21:00 on 09-07-2024 to 14:00 on 10-07-2024 to capture the full diurnal dynamics.

Stem hydraulic capacitance and PLC (Ψ) risk Estimation

We derived apparent stem hydraulic capacitance (*Cs*; mm MPa^{-1}) in situ from paired SCV-Ψ_{STEM} changes during the daylight shrinkage and nocturnal refill windows. For each diel cycle, we computed the slope of the linear relation between SCV (mm) and Ψ_{STEM} (MPa) as follows (Zweifel and Häsler 2001; Meinzer et al. 2003):

$$Cs = (SCV_{MD} - SCV_{PD}) \,/\, (\Psi_{STEM\,MD} - \Psi_{STEM\,PD}) \quad (1)$$

where SCV_{MD} and SCV_{PD} are stem circumference variation at midday and predawn, and $\Psi_{STEM\ MD}$ and $\Psi_{STEM\ PD}$ are stem water potential at midday and predawn, respectively, corresponding to the same measurement phases as the conventional leaf water potential measurements described above.

This *Cs* captures the elastic tissue buffering at the sensor level (tree-scale "apparent" capacitance) and is not a volumetric water content.

Terminal branches (1 m length, 1 cm diameter, 3–5 years old) were harvested once at predawn (tension minimised) from five trees in the studied site during the stress season, immediately placed in water, shaded, and transported moist and insulated. In the laboratory, samples were re-cut under water to restore continuous water columns. Twigs/shoots were sequentially trimmed; water potential of each segment was measured with a Scholander pressure chamber (SKPM 1400, Skye Instruments, UK) prior to conductivity assays. Xylem vulnerability curves were then constructed on excised segments using a high-pressure conductivity flow meter (*HCFM*; (Sperry et al. 1988). For each segment we measured hydraulic conductivity at its prevailing Ψ (*Ks*; kg s^{-1} m^{-1} MPa^{-1}) and maximum conductivity after flushing at 10 kPa (*Kmax*). Percent loss of conductivity was computed as:

$$\mathrm{PLC} = 100(K_{max} - K_S)/K_{max}. \quad (2)$$

Laboratory *PLC*–Ψ data were fitted with the sigmoidal model (Pammenter & Van der Willigen, 1998; Duursma and Choat 2017),

$$\mathrm{PLC} = 100/(1 + \exp(\mathrm{a}(\Psi_{STEM} - \mathrm{b}))) \quad (3)$$

where a is the slope parameter and b is the location parameter representing the water potential at 50% conductivity loss (Ψ_{50}). Both parameters were derived from laboratory vulnerability curves fitted with the fitplc R package (Duursma and Choat 2017), which implements both Weibull (Ogle et al. 2009) and sigmoidal (Pammenter & Van der Willigen, 1998) models. Fitted coefficients for this study were a = -1.45 and b = 0.87 (Table S3; Fig. S2).

Environmental data

In March 2024, an eddy covariance (*EC*) tower (see Table 1 for definitions of symbols and abbreviations) was installed at 1.5 m above the canopy in the thinned *Pinus sylvestris* stand. The instrumentation setup consisted of a three-dimensional sonic anemometer (CSAT3, Campbell Scientific, Logan, UT, USA in PST) measuring (u, v, w) components and sonic temperature at 20 Hz. An open-path infrared gas analyser (LI-7500 in PST, LI-COR Biosciences Inc., Lincoln, NE, USA) provided synchronous CO_2 and H_2O molar densities. Ancillary sensors comprised a four-component net

Table 1 Definition of symbols and abbreviations used repeatedly in the main text

Symbol	Definition	Symbol	Definition
AIC	Akaike information criterion	Ψ_{LEAF}	Leaf water potential (MPa)
BIC	Bayesian information criterion	Ψ_{STEM}	Stem water potential (MPa)
Cs	Stem water capacitance (mm MPa^{-1})	*RH*	Relative humidity (%)
EC	Eddy covariance	*RMSE*	Root mean square error
K_S	Hydraulic conductivity (kg $m^{-1}s^{-1}$ MPa^{-1})	R_N	Net radiation (W m^{-2})
LE	Latent heat flux (evapotranspiration) (W m^{-2})	*SCV*	Stem circumference variation (mm)
MD	Midday	*SLR*	Simple linear regression
MDS	Maximum daily shrinkage (mm)	*SPAC*	Soil-plant-atmosphere continuum
MDE	Maximum daily expansion (mm)	*SWC*	Soil water content (m^3 m^{-3})
PAR	Photosynthetic active radiation (µmol photons m^{-2} s^{-1})	*TWD*	Tree water deficit (mm)
P_{50}	Water potential at which 50% of hydraulic conductivity loss	*VIF*	Variance inflation factor
PLC (Ψ)	Estimated embolism risk (%)	*VPD*	Vapor pressure deficit (Kpa)
PD	Predawn		

radiometer (NR-Lite, Kipp & Zonen, Delft, Netherlands). Two replicated heat-flux plates (HFP01-L, Hukseflux, Netherlands) were installed – one under trees and one under open sky − at 2 cm depth. Soil temperature and moisture probes (EC-5, Decagon Inc., Pullman, EEUU) were installed adjacent to the heat-flux plates at 20 cm depth. Meteorological and soil data were also acquired continuously at high frequency. Raw 20 Hz data were tilt-corrected, despiked, and time-lag optimised in EddyPro 7.0.9 (LI-COR). Quality control followed (Foken and Wichura 1996) flags 0–1; periods with low friction velocity were discarded. Remaining gaps (< 16% of records) were filed with the (Reichstein et al. 2005) marginal distribution approach. A comprehensive description of the data processing steps, error assessment, and quality control procedures is provided in (Perez-Priego et al. 2017).

Statistical analysis

We used linear regression model to evaluate the relationship between Ψ_{STEM} and Ψ_{LEAF} using the base lm function. Model performance was assessed using multiple statistics derived from the summary function, including the coefficient of determination (R^2), adjusted R^2, residual standard error, F-statistic, and associated *p*-value (Fig. 2, Table S1). Each Ψ_{STEM} measurement was paired with the nearest Ψ_{LEAF} measurement in time using a custom nearest-neighbour approach within a 15-minute window to ensure temporal alignment of the data.

Additionally, we computed the Akaike Information Criterion (AIC) and Bayesian Information Criterion (BIC) using the AIC and BIC functions from the base stats package to evaluate model parsimony. All statistical analyses and visualisations were conducted in R, and model assumptions were verified using residual diagnostics.

To evaluate the influence of physiological and environmental variables on stem circumference variation (*SCV*), a linear mixed-effects model was fitted using the lme4 package in R. The model included fixed effects for stem water potential (Ψ_{STEM}), air temperature (*Tair*), vapor pressure deficit (*VPD*), relative humidity (*RH*), and soil water content (*SWC*), with a random intercept for individual trees (tree_id) to account for repeated measurements. The model was fitted using maximum likelihood estimation (REML = FALSE). Statistical significance of fixed effects was assessed using Satterthwaite's approximation for degrees of freedom via the lmerTest package. Model performance was evaluated through residual diagnostics and variance partitioning. Marginal and conditional R^2 values were computed using the MuMIn package, while model assumptions and multicollinearity were examined using the performance and car packages. Model outputs were further organized using broom.mixed for reporting.

To examine the relationships between stem circumference variation at midday (SCV_{MD}) and midday water potential (Ψ_{MD}) as well as midday Ψ-mapped embolism risk, $PLC\ (\Psi_{MD})$, we performed simple linear regression analyses using the base lm function. Here $PLC\ (\Psi_{MD})$ denotes a diagnostic snapshot obtained by mapping in-situ Ψ_{MD} onto the laboratory vulnerability curve. Each relationship was assessed using ordinary least squares (OLS) regression, and model fit was evaluated by the coefficient of determination (R^2) and associated *p*-values.

All analyses were conducted using R version 4.2.2.

Results

Transition to Water-Limited conditions during summer Dry-Down

The Fig. 1 depicts monthly mean diurnal cycles of net radiation (R_N), air temperature (T_{AIR}), relative humidity (*RH*), vapor pressure deficit (*VPD*), near-surface soil temperature (T_S), latent heat flux (*LE*; proxy for evapotranspiration), volumetric soil water content (*SWC*), and stem water potential (Ψ_{STEM}). Following the final late-spring recharge, R_N, T_{air}, and *VPD* rise to early–mid-summer maxima, initiating a pronounced summer dry-down in which *SWC* declines quasi-monotonically through the season. *LE* initially scales with R_N (≈ 20% of available energy) but progressively weakens as *SWC* is depleted; despite persistently high R_N and *VPD*, *LE* reaches a minimum of ≈ 9% of available energy by August, coincident with the most negative Ψ_{STEM} values. T_{SOIL} mirrors *Tair* with attenuation and slight lag, sustaining high evaporative demand but offering little relief to soil moisture.

Concordance between continuous stem and discrete leaf water potentials during a representative summer dry-down day

Continuous stem water potential (Ψ_{STEM}, MPa) was recorded throughout the day using microtensiometers, overlaid with discrete predawn and midday leaf water potential (Ψ_{LEAF}, MPa) obtained with a Scholander-type pressure chamber (Fig. 2A). Both methods resolve the diel trajectory: least-negative values near predawn (≈ −0.5 MPa), followed by a steady morning decline to early-afternoon minima, and partial recovery during the evening. Discrete Ψ_{LEAF} falls on the same declining trend as the continuous Ψ_{STEM} trace; small but systematic offsets are evident—during daylight Ψ_{STEM} tends to be slightly less negative than Ψ_{LEAF} (e.g.,

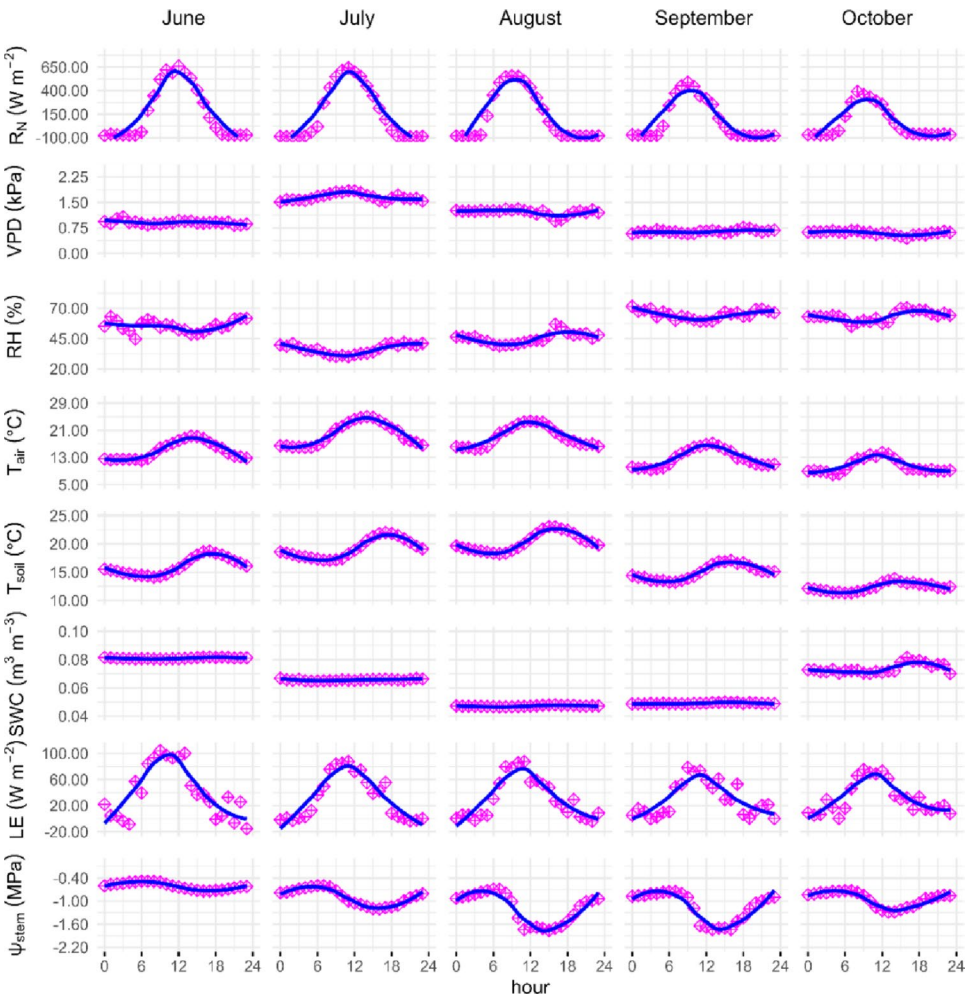

Fig. 1 24-h mean values of microclimatic variables derived from the eddy covariance system measured from June to October in 2024. Abbreviations: Net radiation (R_N; W m^{-2}).Vapour pressure deficit (*VPD*; Kpa), Relative humidity (*RH*; %), Air temperature (*Tair*; ºC), Soil temperature (*Tsoil*; ºC), Soil water content (*SWC*; m^3 m^{-3}), Heta latent flux or evapotranspiration (LE; W m^{-2}) and water potential in stem (Ψ_{STEM}; MPa) in a *Pinus sylvestris* thinned stand located in the Sierra Nevada (Granada, Spain)

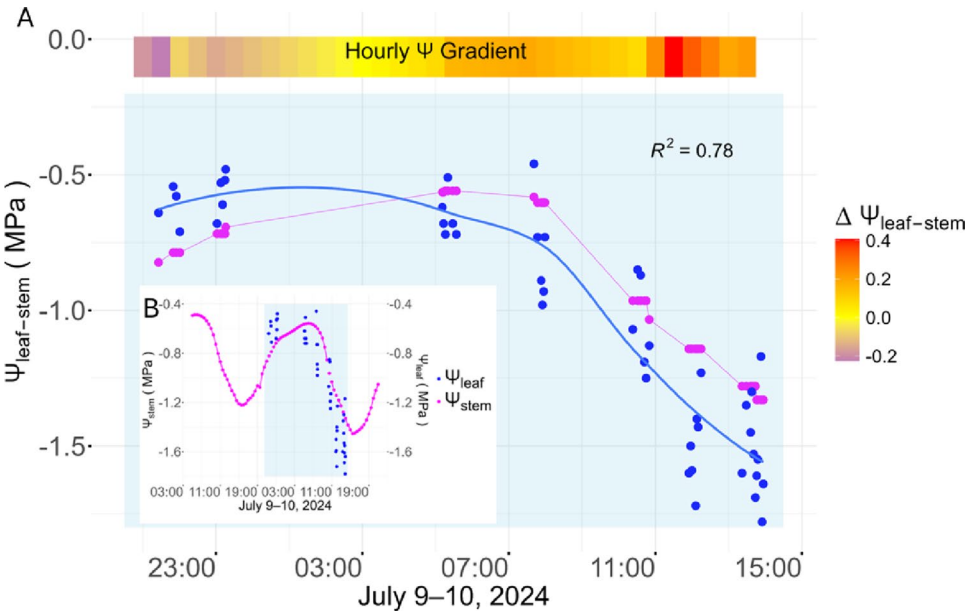

Fig. 2 Figure A shows the hourly mean variation in Ψ between the conventional method (Scholander chamber) and the newer technology (Florapulse microtensiometers) and Figure B shows water potential (Ψ_{STEM}; MPa) measurements recorded by the Florapulse microtensiometers (magenta-coloured points) from July 9 to July 10, 2024 (x-axis) and the measurements from the Scholander pressure chamber (Ψ_{LEAF}; MPa) (blue-coloured points) used to validate the microtensiometer readings over a continuous period in a *Pinus sylvestris* thinned stand located in the Sierra Nevada (Granada, Spain)

~11:00–15:00, $\Psi_{STEM} \approx -1.2$ MPa vs. $\Psi_{LEAF} \approx -1.5$ MPa), whereas in the evening Ψ_{STEM} can be slightly more negative (e.g., ~23:00, $\Psi_{STEM} \approx -0.8$ MPa vs. $\Psi_{LEAF} \approx -0.6$ MPa).

The pairwise differences ($\Psi_{LEAF} - \Psi_{STEM}$, MPa) for all coincident observations within the analysis window shown in (A), annotated by the concurrent rate of change in water potential (dΨ/dt). A quadratic fit explains 78% of the variance ($R^2 = 0.78$; Table S1), indicating a strong, systematic relationship between the two measurement approaches: differences are slightly positive at night (+0.1 to +0.2 MPa), and negative during peak transpiration (−0.3 to −0.6 MPa), (Fig. 2B).

Dynamics of stem and leaf water potential in relation to stem circumference variation

Diurnal trajectories of stem water potential (Ψ_{STEM}) and stem circumference variation (*SCV*) were tightly coupled in both focal trees (Fig. 3). In each case, *SCV* increased overnight to a morning maximum, then declined through the day as stems shrank, while Ψ_{STEM} shifted from least-negative values before dawn to early-afternoon minima and partially recovered toward evening. Midday leaf water potentials (Ψ_{LEAF}) clustered around the time of maximum evaporative demand and were consistently more negative than co-occurring Ψ_{STEM}, reflecting expected within-tree tension gradients. The correspondence between the diel *SCV* pattern and Ψ_{STEM} dynamics was strong (Tree A: $R^2 = 0.57$; Tree B: $R^2 = 0.89$), validating the coherence of the two sensor streams at sub-daily scales. Despite shared phasing, the two individuals differed in magnitude and recovery. Tree A showed larger daytime shrinkage and deeper midday depressions in Ψ_{STEM}, with more limited evening rebound, whereas Tree B exhibited smaller *SCV* excursions and slightly less negative midday Ψ_{STEM} with improved nocturnal re-swelling.

At the seasonal scale (Fig. S1), both trees exhibited a progressive decline in *SCV* from early July to late summer, coinciding with increasingly negative Ψ_{STEM} values. Transient rehydration events in September and October produced short-term *SCV* increases and partial Ψ_{STEM} recovery. Towards late October, both individuals exhibited gradual *SCV* recovery and less negative Ψ_{STEM}, marking the end-of-season rehydration phase and the transition into dormant conditions.

The linear mixed-effects model revealed that all predictors had statistically significant effects on *SCV*. Notably,

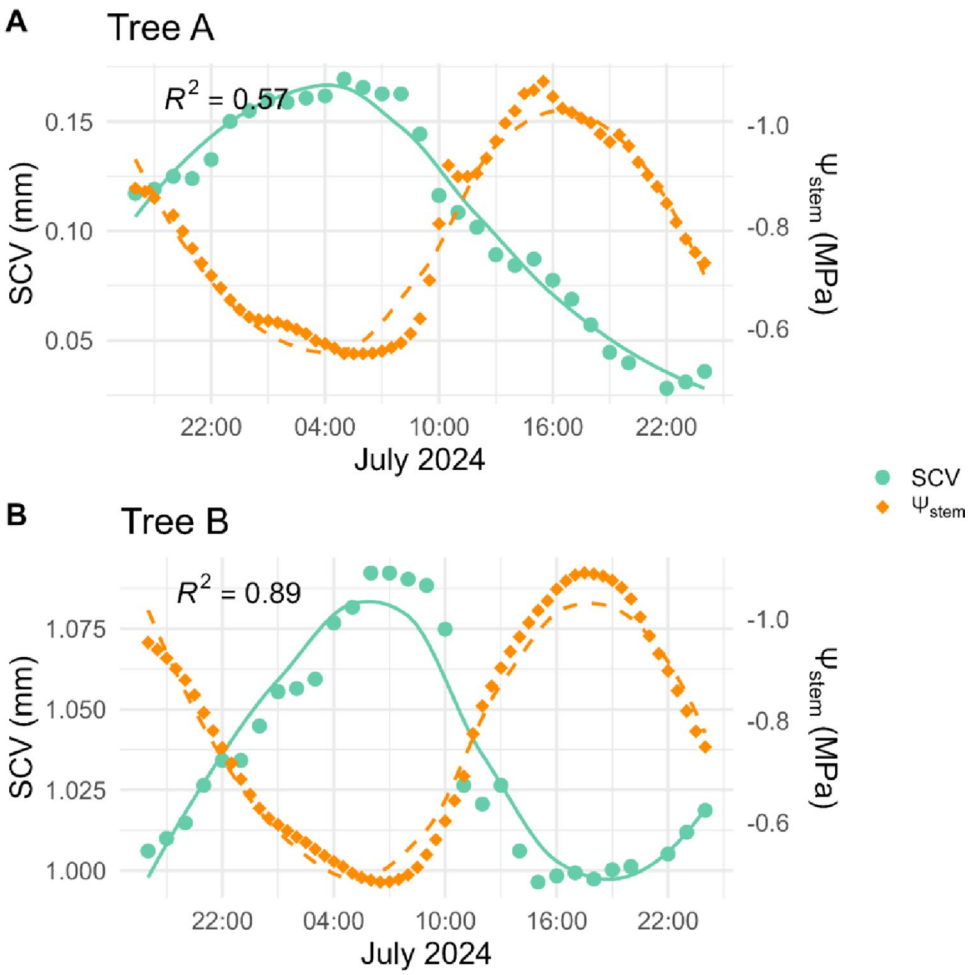

Fig. 3 24-hour comparison between stem circumference variation (*SCV*; mm, expressed as deviation from the initial baseline (0 µm), relative to the start of Ψ_{STEM} monitoring) and stem water potential measured with microtensiometers (Ψ_{STEM}; MPa) in two different trees from July 9th to July 10th of 2024 in a *Pinus sylvestris* thinned stand located in the Sierra Nevada (Granada, Spain). *SCV* is expressed as deviation from the initial baseline (0 mm)

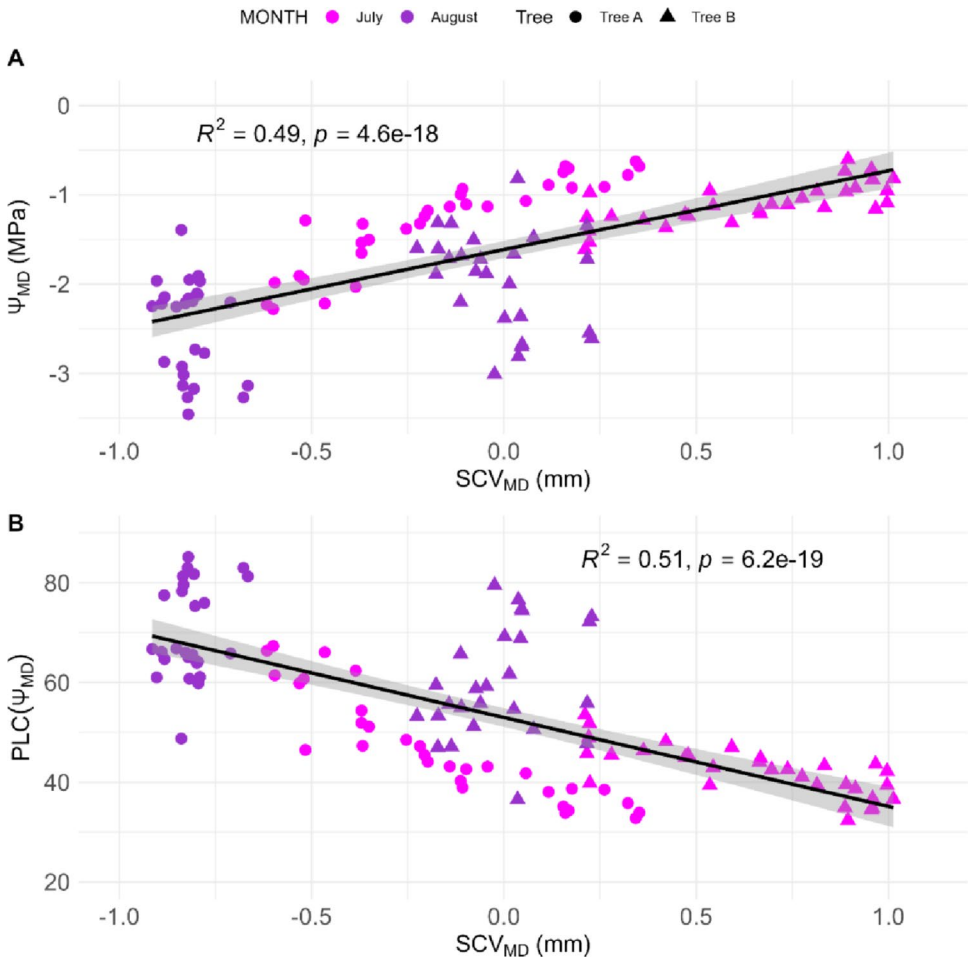

Fig. 4 Panel A shows the relationship between midday stem water potential (Ψ_{MD}; MPa) and stem circumference variation (*SCV*; mm, expressed as deviation from the initial baseline (0 mm), relative to the start of Ψ_{STEM} monitoring) and panel B show the relationship between estimated embolism risk at midday (PLC_{MD} derived PLC (Ψ_{MD}) (Ψ-mapped embolism risk); %) and stem circumference variation (*SCV*; µm) during water stress season (July and August) in a *Pinus sylvestris* thinned stand located in the Sierra Nevada (Granada, Spain). Each point represents one day and one tree

SCV increased with higher Ψ_{STEM}, *Tair*, *VPD*, *RH*, and *SWC* (all $p<0.05$), with *SWC* showing the strongest effect. The model explained 98.8% of the total variance (conditional R^2), indicating strong explanatory power driven largely by between-tree differences. Fixed effects alone accounted for 10.5% of the variance (marginal R^2). Residuals were approximately normally distributed and homoscedastic, and multicollinearity among predictors was within acceptable limits (VIF < 3.5; Table S2).

Effect of stem circumference variation on midday stem water potential and Ψ-mapped embolism risk

Midday stem shrinkage covaried tightly with stem water potential throughout the dry-down (Fig. 4). A linear mixed-effects model (tree as a random intercept) revealed a strong negative association between midday stem circumference variation (SCV_{MD}) and midday stem water potential (Ψ_{MD}): larger shrinkage coincided with more negative Ψ_{MD} (marginal $R^2 = 0.49$, $p<0.001$; Fig. 4A). This relationship was consistent across individuals and dates, with July observations spanning moderate shrinkage and Ψ_{MD} values, and August observations clustering toward greater shrinkage and more negative Ψ_{MD}, reflecting progressive seasonal drying.

Midday Ψ-mapped embolism risk, $PLC\ (\Psi_{MD})$, estimated by mapping in-situ Ψ_{MD} onto laboratory vulnerability curves increased with the magnitude of SCV_{MD} (marginal $R^2 = 0.51$, $p<0.001$; Fig. 4B), indicating that days with greater stem contraction also exhibited higher estimated embolism risk. The trend was robust across trees; with August points shifted toward higher embolism risks relative to July.

Complementary bivariate analyses across the full June–October period (Fig. S3) reinforced these relationships. Midday Ψ_{MD} became progressively more negative with increasing SCV_{MD} ($R^2 = 0.29$, $p<0.001$; Fig. S3A), and $PLC(\Psi_{MD})$ increased with increasing SCV_{MD} ($R^2 = 0.29$, $p<0.001$; Fig. S3B).

Discussion

Continuous microtensiometer–dendrometer monitoring effectively resolved in situ stem hydraulic dynamics across the seasonal dry-down. The coordination among stem capacitance (C_S), estimated embolism risk, $PLC\ (\Psi)$, obtained

by mapping in-situ Ψ_{STEM} onto laboratory vulnerability curves, and water potential (Ψ_{STEM}) underscores fundamental trade-offs governing drought response and resilience. Progressive stem contraction reflected the depletion of elastic water reserves that buffer transpiration-driven tension, while higher *PLC (Ψ)* estimates are consistent with elevated cavitation risk; our data do not track embolism formation or repair. These dynamics highlight the dual role of the stem as both a transient water capacitor and a hydraulic bottleneck during drying. Consistent with previous studies (Pfautsch et al., 2015; Steppe et al., 2015; Zweifel et al. 2005), our findings indicate that maintaining stem capacitance can delay hydraulic failure by sustaining short-term water fluxes, although recovery upon rehydration likely involves elastic refilling rather than xylem repair.

Methodologically, we present an in situ derivation of stem hydraulic capacitance (*Cs*) from paired *SCV*–Ψ_{STEM} time series—representing, to our knowledge, the first demonstration in a conifer—thereby linking internal water storage, xylem vulnerability, and tree-level water dynamics under drought. Traditional approaches to estimate *Cs* typically rely on destructive laboratory methods, such as pressure–volume curves or dehydration of excised branches, which provide static or integrated values under controlled conditions (Meinzer et al. 2003). In contrast, our approach quantifies *Cs* continuously and non-destructively from high-resolution dendrometer records, directly coupled with stem water potential measurements. By resetting *SCV* to zero at the start of the measurement period, we track stem circumference fluctuations relative to the initial measurement, capturing water-related changes in diameter. We note that this approach does not fully isolate reversible shrinkage from growth, and therefore *Cs* should be interpreted as an integrated measure of water storage dynamics rather than strictly reversible changes, consistent with the limitations of our methodology. This dynamic framework captures diel and seasonal elasticity of living tissues in situ, providing a level of temporal and physiological resolution unattainable with traditional methods.

The novelty of this approach lies in its ability to resolve capacitance dynamics continuously under natural environmental variation, revealing how water storage modulates short-term hydraulic buffering during drought progression. Nonetheless, because *SCV* integrates both xylem and elastic tissue responses, absolute *Cs* values may slightly overestimate xylem-specific capacitance. Moreover, structural and anatomical factors—such as bark thickness, phloem elasticity, and species-specific wood density—can influence the magnitude of reversible *SCV*, underscoring the need for species-level calibration and comparative validation across sites.

Performance of in-situ microtensiometry and coherence with dendrometry

Continuous stem water potential (Ψ_{STEM}) measured by microtensiometers closely matched independent leaf water-potential (Ψ_{LEAF}) from a Scholander-type pressure chamber ($R^2 = 0.78$, Fig. 2), and covaried tightly with sub-daily stem circumference variation (*SCV*, Fig. 3), validating their accuracy under field conditions(Scholander et al. 1965; Zweifel et al. 2000). Systematic offsets between Ψ_{LEAF} and Ψ_{STEM}—less negative Ψ_{STEM} during peak transpiration and slightly more negative Ψ_{STEM} during early recovery—are physiologically expected due to transient axial gradients and the non-instantaneous equilibration among elastic tissues, xylem conduits, and leaves during changing evaporative demand (Jarvis 1976; Meinzer et al. 2003). Slightly more negative Ψ_{STEM} overnight (≈0.1 MPa) under low *VPD* indicates residual xylem tension and osmotic gradients sustaining minor disequilibria during periods of minimal hydraulic activity (Caird et al. 2007).

The synchronized diel cycles—daytime *SCV* shrinkage with nocturnal re-expansion coinciding with Ψ_{STEM} decline and recovery—confirm tight coupling between xylem tension and elastic storage dynamics. As the seasonal dry-down progressed, midday Ψ_{STEM} became increasingly negative, daytime *SCV* amplitudes enlarged, and nocturnal refilling declined, consistent with rising atmospheric demand (*VPD*) and reduced soil water availability (*SWC*) constraining rehydration (Meinzer et al. 2008). Inter-individual variation in *SCV* amplitude suggests different access to water or storage capacity, justifying the mixed-effects approach.

The non-linear relationship between Ψ_{LEAF} and Ψ_{STEM} ($R^2 = 0.78$, Fig. 2) highlights phase-dependent stem capacitance. During nocturnal refilling, Ψ_{LEAF} was slightly higher (+0.1 to +0.2 MPa) due to faster equilibration of leaves with moist soil, whereas daytime offsets (–0.3 to −0.6 MPa) reflect limited release of stored stem water under high *VPD* (Choat et al. 2018; Grossiord, Ulrich, et al., 2020). Such phase-specific lags buffer transient hydraulic stress and delay cavitation (Cochard et al. 1992; De Swaef et al. 2015).

These findings extend previous applications of tensiometry and dendrometry by demonstrating stable, high-resolution Ψ_{STEM} sensing in conifer sapwood, with strong agreement to pressure-chamber benchmarks under field drought (Scholander et al. 1965; Novick et al. 2022). Combined with *SCV*, microtensiometers offer a non-destructive means to resolve diel and seasonal hydraulic dynamics in tall forest trees.

Overlaying Ψ_{STEM} with *SCV* time series showed that stem-level water-potential fluctuations directly drive reversible circumference changes—daytime contractions and nocturnal expansion—mirroring the inverse *SCV*–*Ψ*

relationship described by Zweifel et al. (2000) and Steppe (2018). Strong correlations (Fig. 3) indicate that Ψ_{STEM} captures most of the hydraulic signal underlying *SCV*, validating *SCV* as a reliable proxy for midday water potential (Ψ_{MD}) when tensiometry is impractical (Zweifel et al. 2000; Ziegler et al. 2024). Reversible *SCV* during dry periods reflects depletion of elastic water reserves under high evaporative demand (Oberhuber et al., 2023), with partial recovery in early autumn signaling stem rehydration when soil moisture improves (Fig. S1).

Mixed-effects modeling revealed that *SCV* is governed by Ψ_{STEM} and microclimatic drivers (T_{AIR}, *VPD*, *RH*, and *SWC*) with the latter exerting the strongest fixed effect. The high conditional R^2 (98.8%) underscores inter-tree structural differences, while the marginal R^2 (10.5%) reflects environmental modulation (Table S2). Together, these results show that, in dry mountain environments, integrating continuous Ψ_{STEM} measurements with *SCV* and microclimate monitoring provides a robust, non-destructive toolkit for detecting early hydraulic dysfunction and assessing drought vulnerability in mature conifers (Meinzer et al. 2009; Bourbia et al. 2025).

SCV as an operational proxy for hydraulic status and embolism risk

Our results show that midday stem shrinkage (SCV_{MD}) captures key variation in hydraulic status and impairment at daily to seasonal scales. Specifically, SCV_{MD} covaried negatively with midday stem water potential (Ψ_{MD}; marginal $R^2 = 0.49$, Fig. 4A) and positively with midday Ψ-mapped embolism risk, *PLC* (Ψ_{MD}) (marginal $R^2 = 0.51$, Fig. 4B), indicating that larger midday contraction corresponds to more negative xylem tensions and higher estimated embolism risk during peak atmospheric demand. Physiologically, this is expected: daytime withdrawal of water from elastic tissues to sustain transpiration reduces stem radius, while nocturnal rehydration drives partial swelling; the amplitude of this reversible cycle scales with the underlying water-potential gradients along the soil–plant–atmosphere continuum Zweifel et al. 2000; Steppe et al. 2006). By leveraging these dynamics, SCV_{MD} provides a practical, non-destructive proxy where direct tensiometry is infeasible (e.g., tall canopies), and complements discrete pressure-chamber measurements by filling sub-daily gaps with high temporal resolution. This coupling persisted throughout the summer drought—period marked by sustained high air temperatures and elevated vapor pressure deficits (Fig. 1) that intensified transpirational demand (McDowell et al. 2008; Novick et al. 2016) underscoring SCV_{MD} sensitivity as an integrative indicator of water potential when radial growth is minimal (Steppe et al. 2006).

Relative to other indirect indicators (e.g., sap flow or canopy fluxes), *SCV* offers two advantages for diagnosing hydraulic stress in situ: (i) it directly indexes the local balance between elastic water release and refilling in the measured stem segment, and (ii) it responds rapidly to shifts in Ψ, thereby tracking both daytime drawdown and the degree of nocturnal recovery. Nevertheless, several caveats merit emphasis when generalizing *SCV* as a proxy. First, *SCV* integrates both reversible (hydration) and irreversible (growth) components; careful growth–shrinkage separation and thermal-drift correction are essential to avoid biasing hydraulic inferences. Second, bark thickness, wood density, and tissue anisotropy can modulate the magnitude of *SCV* for a given change in Ψ, implying that proxy relationships (SCV_{MD}–Ψ_{MD}; SCV_{MD} –$PLC(\Psi_{MD})$) require site- and species-specific calibration before management thresholds are inferred. Third, environmental context matters: elevated *VPD* can amplify *SCV* independently of large changes in soil water content, while low *SWC* constrains nocturnal refilling and progressively shifts observations toward larger SCV_{MD} and higher *PLC* (Ψ_{MD}) (i.e., higher estimated embolism risk) as the dry-down advances.

Considering the above, the observed negative correlation between SCV_{MD} and *PLC* (Ψ_{MD}) ($R^2 = 0.51$, $p < 0.001$; Fig. 4B) likely reflects their shared dependence on stem water potential, as both stem shrinkage and Ψ-mapped embolism risk, PLC(Ψ), are governed by declining xylem pressure. Nevertheless, this strong relationship underscores that *SCV* captures integrated hydraulic responses, serving as a practical, non-destructive indicator of drought-induced embolism risk (Meinzer et al. 2001; Bartlett et al. 2012). As midday vapor pressure deficit increased and soil water content declined (Fig. 1), trees faced steeper vapor pressure gradients that promoted tension-induced cavitation, directly mirrored in greater *PLC* (Ψ_{MD}) estimates at more negative SCV_{MD}. During periods of growth cessation, when stem-diameter changes predominantly reflect elastic tissue dehydration and rehydration rather than irreversible cambial expansion (Zweifel et al. 2000; Steppe et al. 2006), SCV_{MD} therefore serves as both a real-time proxy for hydraulic pathway embrittlement and an early warning of approaching critical thresholds (Oberhuber et al. 2014).

Taken together, these considerations argue for using SCV_{MD} as an operational proxy—ground-truthed against Ψ and vulnerability curves where possible—rather than as a universal surrogate. In our conifer stand, the consistency of *SCV*–Ψ phasing, the agreement with pressure-chamber benchmarks, and the emergent *SCV–PLC* (Ψ) relationship collectively support SCV_{MD} as a useful indicator of hydraulic status and vulnerability risk during peak summer drought, while underscoring the need for calibration when extending to other sites or species. Integrating such continuous *SCV*

metrics into ecohydrological and vegetation-mortality models should substantially improve our ability to forecast tree drought responses and mortality risk under escalating climatic extremes (Zweifel et al. 2005).

Capacitance–embolism risk trade-off and consequences for seasonal hydraulics

Across the summer dry-down, estimated embolism risk at midday, *PLC* (Ψ_{MD}), increased from moderate to high levels, while stem hydraulic capacitance (*Cs*) declined markedly. revealing a clear inverse relationship between internal water buffering and conduit safety (risk context). Mechanistically, under elevated embolism risk (higher *PLC* (Ψ)), both the hydraulically connected storage and the efficiency of transfer from elastic tissues to the transpiration stream may be reduced, which is consistent with our observed decline in apparent *Cs* even as atmospheric demand intensifies. Stem shrinkage primarily reflects water release from elastic tissues, such as bark and parenchyma, whereas stiff xylem conduits contribute little to diameter changes due to their rigidity. The relationship between stem shrinkage and water release is therefore not strictly linear and may vary seasonally or among tissues with different elasticity. Consequently, our in situ *Cs* metric differs from traditional capacitance measurements from excised branches or pressure–volume curves, representing a tree-level proxy for integrated water storage dynamics rather than a quantitative measure of total water loss.

This decoupling between xylem water release and stem shrinkage likely contributes to the apparent decline in capacitance under severe drought. This mechanistic link is further supported by the low soil water content observed during the summer dry-down (Fig. 1), which exacerbates xylem tension and elevates embolism risk. While sap flow measurements were not available to directly quantify water transport efficiency, the high-resolution *SCV*–Ψ_{STEM} time series are consistent with elevated embolism risk contributing to the observed reduction in apparent stem capacitance; note that embolism formation/repair was not directly tracked. Thus, both hydraulic limitation and depletion of elastic water storage likely act in concert to reduce *Cs* during prolonged drought (Salomón et al. 2017). This dynamic helps explain the progressive enlargement of daytime stem shrinkage, the increasingly incomplete nocturnal re-swelling (Fig. S1), and the deepening midday Ψ_{STEM} minima observed through late summer. These patterns are mirrored by declines in normalized maximum daily shrinkage (MDS_n), which reflects increasing tree water deficit (*TWD*) (Fig. S4), and support the interpretation that incomplete nightly rehydration results from the combined effects of rising xylem tension and hydraulic limitation under drought. In parallel, canopy latent energy (*LE*) measured by eddy covariance attenuated during periods of higher *PLC* (Ψ) estimates, consistent with stomatal regulation and photosynthetic traits in response to declining hydraulic supply and rising vapor-pressure deficit (*VPD*) (Chhajed et al. 2024). Low soil-water content (*SWC*) further constrained refilling at night, reinforcing the seasonal decline in apparent C_S.

Our data highlight the tight coupling between hydraulic limitation and stem water storage dynamics in Pinus sylvestris. Peak drought stress drove higher midday Ψ-mapped embolism risk, *PLC* (Ψ_{MD}), and a sharp decline in stem hydraulic capacitance (*Cs*), consistent with elevated embolism risk and depletion of elastic water reserves, including dehydration of living tissues and shrinkage of xylem parenchyma cells (Hacke and Sperry 2001; Zweifel et al. 2005; Steppe et al. 2006; McDowell et al. 2008; Hölttä et al. 2009; Bartlett et al. 2012). Reduced capacitance limits internal water buffering, accelerating the progression toward critical water potentials (Meinzer et al. 2003). Following the drought peak, *PLC* (Ψ_{MD}) estimates declined and *Cs* stabilized, indicating tension relief (less-negative Ψ) and partial replenishment of internal water storage as soil moisture improved; this does not demonstrate refilling of previously embolized xylem consistent with recent findings that stress duration and cumulative water deficit affect post-stress recovery (Knüver et al. 2025). These seasonal dynamics reinforce the utility of high-resolution dendrometer measurements as integrative indicators of tree water stress and vulnerability (Scholz et al. 2008; Oberhuber et al. 2015).

The emerging C_S –*PLC* (Ψ_{MD}) pattern situates our stand within classic safety–efficiency trade-offs: where structural or management-driven increases in hydraulic efficiency can coincide with heightened vulnerability to embolism (less negative P_{50}) (Choat et al. 2008, 2018; Brodribb and Cochard 2009; Rosner et al. 2019). In this framework, C_S serves as the first buffer against rapid Ψ declines, but its protective capacity erodes as embolism risk increase, narrowing the window for safe stomatal operation and accelerating the transition to canopy-scale water-use limitation. Methodologically, our in situ estimation of C_S from paired *SCV*–Ψ_{STEM} time series provides a high-resolution view of this trade-off in mature conifers, complementing Ψ-mapped embolism risk, PLC(Ψ), inferred from vulnerability curves. We note, however, that species-specific bark/wood properties and the separation of growth versus shrinkage can modulate apparent C_S; highlighting the need for site-level calibration and consideration for thermal drift when applying these relationships beyond the present stand.

Conclusions

Continuous microtensiometer–dendrometer monitoring resolved diel-to-seasonal stem water relations in a mature *Pinus sylvestris* stand. Apparent stem hydraulic capacitance (*Cs*), derived in situ from paired SCV–Ψ_{STEM} trajectories, declined through the summer dry-down, while midday Ψ-mapped embolism risk, *PLC* (Ψ_{MD}), increased—an inverse pattern consistent with a capacitance–risk trade-off under drought. Midday stem shrinkage (SCV_{MD}) covaried with Ψ_{MD} and with *PLC* (Ψ_{MD}), indicating that SCV_{MD} is a practical, non-destructive proxy of hydraulic status and estimated embolism risk where tensiometry is impractical. Attenuation of canopy latent energy (*LE*) during late summer coincided with more negative Ψ and lower *Cs*, linking internal hydraulics to ecosystem flux responses.

Methodologically, our framework extends microtensiometry to operational forestry and demonstrates the value of coupling it with high-resolution dendrometry to quantify *Cs* in situ. Importantly, *PLC* was not retrieved continuously; instead, *PLC* (Ψ) was estimated at diagnostic intervals by mapping in-situ Ψ onto laboratory vulnerability curves, and thus should be interpreted strictly as a Ψ-based risk diagnostic rather than evidence of embolism formation or repair. Future work should add direct embolism observations (e.g., microCT, acoustic emissions) and growth–shrinkage separation refinements to tighten causal inference. Together, these results support integrating *SCV*- and Ψ-based indicators into nowcasting and decision tools for drought-aware, physiology-informed forest management.

Acknowledgements We thank Michael Santiago (FloraPulse, CA, USA) for providing the microtensiometer probes. Also, special thanks go to E.P. Sánchez-Cañete, A.S. Kowalski and E. Cardel for scientific support.

Authors contribution statements Both authors contributed equally to this work (Writing – original draft, Investigation, Analyses and Conceptualization). OPP secured the Funding Acquisition.

Funding Funding for open access publishing: Universidad de Córdoba/CBUA. This research was collaboratively funded by the following projects: REMEDIO (PID2021-128463OB-I00), EVIDENCE (Ref: 2822/2021), and NextGen EU (BIOD22-00033-17-PPCB).

Declarations

Conflict of interest The authors declare that they have no conflict of interest.

References

Allen CD, Macalady AK, Chenchouni H, Bachelet D, McDowell N, Vennetier M, Kitzberger T, Rigling A, Breshears DD, Hogg EH, Ted), Gonzalez P, Fensham R, Zhang Z, Castro J, Demidova N, Lim JH, Allard G, Running SW, Semerci A, Cobb N (2010) A global overview of drought and heat-induced tree mortality reveals emerging climate change risks for forests. For Ecol Manag 259(4):660–684. https://doi.org/10.1016/j.foreco.2009.09.001

Anderegg WR, Klein T, Bartlett M, Sack L, Pellegrini AF, Choat B, Jansen S (2016) Meta-analysis reveals that hydraulic traits explain cross-species patterns of drought-induced tree mortality across the Globe. Proc Natl Acad Sci 113(18):5024–5029

Arend M, Link RM, Patthey R, Hoch G, Schuldt B, Kahmen A (2021) Rapid hydraulic collapse as cause of drought-induced mortality in conifers. Proc Natl Acad Sci 118(16):e2025251118

Bartlett MK, Scoffoni C, Sack L (2012) The determinants of leaf turgor loss point and prediction of drought tolerance of species and biomes: A global meta-analysis. Ecol Lett 15(5):393–405. https://doi.org/10.1111/j.1461-0248.2012.01751.x

Blanco V, Kalcsits L (2021) Microtensiometers accurately measure stem water potential in Woody perennials. Plants 10(12). https://doi.org/10.3390/plants10122780

Bourbia I, Yates LA, Brodribb TJ (2025) Using long-term field data to quantify water potential regulation in response to VPD and soil moisture in a conifer tree. New Phytol 246(3):911–923

Brodribb TJ, Cochard H (2009) Hydraulic failure defines the recovery and point of death in water-stressed conifers. Plant Physiol 149(1):575–584. https://doi.org/10.1104/pp.108.129783

Caird MA, Richards JH, Donovan LA (2007) Nighttime stomatal conductance and transpiration in C3 and C4 plants. In *Plant Physiology* (Vol. 143, Issue 1, pp. 4–10). American Society of Plant Biologists. https://doi.org/10.1104/pp.106.092940

Chhajed SS, Wright IJ, Perez-Priego O (2024) Theory and tests for coordination among hydraulic and photosynthetic traits in co-occurring Woody species. New Phytol. https://doi.org/10.1111/nph.19987

Choat B, Cobb AR, Jansen S (2008) Structure and function of bordered pits: New discoveries and impacts on whole-plant hydraulic function. In *New Phytologist* (Vol. 177, Issue 3, pp. 608–626). https://doi.org/10.1111/j.1469-8137.2007.02317.x

Choat B, Brodribb TJ, Brodersen CR, Duursma RA, López R, Medlyn BE (2018) Triggers of tree mortality under drought. In *Nature* (Vol. 558, Issue 7711, pp. 531–539). Nature Publishing Group. https://doi.org/10.1038/s41586-018-0240-x

Cochard H, Bréda N, Granier A, Aussenac G (1992) Vulnerability to air embolism of three European oak species (Quercus Petraea (Matt) Liebl, Q pubescens Willd, Q Robur L). Annales des sciences forestières, vol 49. EDP Sciences, pp 225–233. 3

De Swaef T, De Schepper V, Vandegehuchte MW, Steppe K (2015) Stem diameter variations as a versatile research tool in ecophysiology. Tree Physiol 35(10):1047–1061

Dietrich L, Zweifel R, Kahmen A (2018) Daily stem diameter variations can predict the canopy water status of mature temperate

trees. Tree Physiol 38(7):941–952. https://doi.org/10.1093/treephys/tpy023
Duursma RA, Choat BA (2017) fitplc-an R package to fit hydraulic vulnerability curves. J Plant Hydraulics 4:e002
Foken T, Wichura B (1996) Tools for quality assessment of surface-based flux measurements. Agric for Meteorol 78(1–2):83–105
Grossiord C, Ulrich DE, Vilagrosa A (2020) Controls of the hydraulic safety–efficiency trade-off. Tree Physiol 40(5):573–576
Haberstroh S, Werner C, Grün M, Kreuzwieser J, Seifert T, Schindler D, Christen A (2022) Central European 2018 hot drought shifts Scots pine forest to its tipping point. Plant Biol 24(7):1186–1197. https://doi.org/10.1111/plb.13455
Haberstroh S, Scarpa F, Seeger S, Christen A, Werner C (2025) Continuous stem water potential measurements of a Diffuse-Porous tree species offer new insights into tree water relations. Ecohydrology 18(1). https://doi.org/10.1002/eco.2761
Hacke UG, Sperry JS (2001) Functional and ecological xylem anatomy. Perspect Plant Ecol Evol Syst 4(2):97–115
Haeni M, Knüsel S, Peters RL, Zweifel R (2020) treenetproc–clean, process and visualise dendrometer data. *R Package Version 0.1*, *4*
Hölttä T, Cochard H, Nikinmaa E, Mencuccini M (2009) Capacitive effect of cavitation in xylem conduits: results from a dynamic model. Plant Cell Environ 32(1):10–21. https://doi.org/10.1111/j.1365-3040.2008.01894.x
Jarvis P (1976) The interpretation of the variations in leaf water potential and stomatal conductance found in canopies in the field. Philosophical Trans Royal Soc Lond B Biol Sci 273(927):593–610
Knüsel S, Peters RL, Haeni M, Wilhelm M, Zweifel R (2021) Processing and extraction of seasonal tree physiological parameters from stem radius time series. Forests 12(6). https://doi.org/10.3390/f12060765
Knüver T, Bär A, Hamann E, Zuber M, Mayr S, Beikircher B, Ruehr NK (2025) Stress dose explains drought recovery in Norway Spruce. Front Plant Sci 16:1542301
Lakso AN, Santiago M, Stroock AD (2022) Monitoring stem water potential with an embedded microtensiometer to inform irrigation scheduling in fruit crops. Horticulturae 8(12). https://doi.org/10.3390/horticulturae8121207
Martínez-Vilalta J, Poyatos R, Aguadé D, Retana J, Mencuccini M (2014) A new look at water transport regulation in plants. New Phytol 204(1):105–115. https://doi.org/10.1111/nph.12912
McDowell N, Pockman WT, Allen CD, Breshears DD, Cobb N, Kolb T, Plaut J, Sperry J, West A, Williams DG, Yepez EA (2008) Mechanisms of plant survival and mortality during drought: Why do some plants survive while others succumb to drought? In *New Phytologist* (Vol. 178, Issue 4, pp. 719–739). https://doi.org/10.1111/j.1469-8137.2008.02436.x
Meinzer FC, Goldstein G, Andrade JL (2001) Regulation of water flux through tropical forest canopy trees: do universal rules apply? Tree Physiol 21(1):19–26
Meinzer FC, James SA, Goldstein G, Woodruff D (2003) Whole-tree water transport scales with sapwood capacitance in tropical forest canopy trees. Plant Cell Environ 26(7):1147–1155. https://doi.org/10.1046/j.1365-3040.2003.01039.x
Meinzer FC, Woodruff DR, Domec JC, Goldstein G, Campanello PI, Gatti MG, Villalobos-Vega R (2008) Coordination of leaf and stem water transport properties in tropical forest trees. Oecologia 156(1):31–41. https://doi.org/10.1007/s00442-008-0974-5
Meinzer FC, Johnson DM, Lachenbruch B, McCulloh KA, Woodruff DR (2009) Xylem hydraulic safety margins in Woody plants: coordination of stomatal control of xylem tension with hydraulic capacitance. Funct Ecol 23(5):922–930. https://doi.org/10.1111/j.1365-2435.2009.01577.x
Novick KA, Ficklin DL, Stoy PC, Williams CA, Bohrer G, Oishi AC, Papuga SA, Blanken PD, Noormets A, Sulman BN (2016) The increasing importance of atmospheric demand for ecosystem water and carbon fluxes. Nat Clim Change 6(11):1023–1027
Novick KA, Ficklin DL, Baldocchi D, Davis KJ, Ghezzehei TA, Konings AG, MacBean N, Raoult N, Scott RL, Shi Y (2022) Confronting the water potential information gap. Nat Geosci 15(3):158–164
Oberhuber W, Gruber A, Kofler W, Swidrak I (2014) Radial stem growth in response to microclimate and soil moisture in a drought-prone mixed coniferous forest at an inner alpine site. Eur J for Res 133(3):467–479. https://doi.org/10.1007/s10342-013-0777-z
Oberhuber W, Kofler W, Schuster R, Wieser G (2015) Environmental effects on stem water deficit in co-occurring conifers exposed to soil dryness. Int J Biometeorol 59(4):417–426. https://doi.org/10.1007/s00484-014-0853-1
Ogle K, Barber JJ, Willson C, Thompson B (2009) Hierarchical statistical modeling of xylem vulnerability to cavitation: methods. New Phytol 182(2):541–554. https://doi.org/10.1111/j.1469-8137.2008.02760.x
Pagay V (2022) Evaluating a novel microtensiometer for continuous trunk water potential measurements in field-grown irrigated grapevines. Irrig Sci 40(1):45–54. https://doi.org/10.1007/s00271-021-00758-8
Pammenter NW, vd, Van der Willigen C (1998) A mathematical and statistical analysis of the curves illustrating vulnerability of xylem to cavitation. Tree Physiol 18(8–9):589–593
Perez-Priego O, El-Madany TS, Migliavaca M, Kowalski AS, Jung M, Carrara A, Kolle O, Martín MP, Pacheco-Labrador J, Moreno G, Reichstein M (2017) Evaluation of eddy covariance latent heat fluxes with independent lysimeter and sapflow estimates in a mediterranean Savannah ecosystem. Agric for Meteorol 236:87–99. https://doi.org/10.1016/j.agrformet.2017.01.009
Peters RL, Basler D, Zweifel R, Steger DN, Zhorzel T, Zahnd C, Hoch G, Kahmen A (2025) Normalized tree water deficit: an automated dendrometer signal to quantify drought stress in trees. New Phytol. https://doi.org/10.1111/nph.70266
Reichstein M, Falge E, Baldocchi D, Papale D, Aubinet M, Berbigier P, Bernhofer C, Buchmann N, Gilmanov T, Granier A, Grünwald T, Havránková K, Ilvesniemi H, Janous D, Knohl A, Laurila T, Lohila A, Loustau D, Matteucci G, Valentini R (2005) On the separation of net ecosystem exchange into assimilation and ecosystem respiration: Review and improved algorithm. In *Global Change Biology* (Vol. 11, Issue 9, pp. 1424–1439). https://doi.org/10.1111/j.1365-2486.2005.001002.x
Rosner S, Johnson DM, Voggeneder K, Domec JC (2019) The conifercurve: fast prediction of hydraulic conductivity loss and vulnerability to cavitation. Ann for Sci 76(3). https://doi.org/10.1007/s13595-019-0868-1
Salomón RL, Limousin JM, Ourcival JM, Rodríguez-Calcerrada J, Steppe K (2017) Stem hydraulic capacitance decreases with drought stress: implications for modelling tree hydraulics in the mediterranean oak Quercus ilex. Plant Cell Environ 40(8):1379–1391. https://doi.org/10.1111/pce.12928
Schmied G, Hilmers T, Uhl E, Pretzsch H (2022) The past matters: previous management strategies modulate current growth and drought responses of Norway Spruce (Picea abies H. Karst). Forests 13(2). https://doi.org/10.3390/f13020243
Scholander PF, Bradstreet ED, Hemmingsen EA, Hammel HT (1965) Sap pressure in vascular plants: negative hydrostatic pressure can be measured in plants. Science 148(3668):339–346
Scholz FC, Bucci SJ, Goldstein G, Meinzer FC, Franco AC, Miralles-Wilhelm F (2008) Temporal dynamics of stem expansion and contraction in savanna trees: withdrawal and recharge of stored water. Tree Physiol 28(3):469–480
Scholz FG, Phillips NG, Bucci SJ, Meinzer FC, Goldstein G (2011) Hydraulic capacitance: biophysics and functional significance of

internal water sources in relation to tree size. Size-and age-related changes in tree structure and function. Springer, pp 341–361
Senf C, Buras A, Zang CS, Rammig A, Seidl R (2020) Excess forest mortality is consistently linked to drought across Europe. Nat Commun 11(1). https://doi.org/10.1038/s41467-020-19924-1
Sperry JS, Donnelly JR, Tyree MT (1988) A method for measuring hydraulic conductivity and embolism in xylem. Plant Cell Environ 11(1):35–40
Spinoni J, Vogt JV, Naumann G, Barbosa P, Dosio A (2018) Will drought events become more frequent and severe in europe? Int J Climatol 38(4):1718–1736
Steppe K (2018) The potential of the tree water potential. Tree Physiol 38(7):937–940
Steppe K, De Pauw DJW, Lemeur R, Vanrolleghem PA (2006) A mathematical model linking tree Sap flow dynamics to daily stem diameter fluctuations and radial stem growth. Tree Physiol 26(3):257–273
Thomas TH (1997) Physiological Plant Ecology. Edited by Walter Larcher
Tyree MT, Zimmermann MH (2002) Xylem structure and the ascent of Sap. Springer Science & Business Media
Wang X, Zhang Q (2023) Interspecific differences of stem diameter variations in response to water conditions for six tree species in Northeast China. Forests 14(4). https://doi.org/10.3390/f14040805
Ziegler Y, Grote R, Alongi F, Knüver T, Ruehr NK (2024) Capturing drought stress signals: the potential of dendrometers for monitoring tree water status. Tree Physiol 44(12):tpae140
Zweifel R, Häsler R (2001) Dynamics of water storage in mature subalpine Picea abies: Temporal and Spatial patterns of change in stem radius. Tree Physiol 21(9):561–569
Zweifel R, Item H, Häsler R (2000) Stem radius changes and their relation to stored water in stems of young Norway Spruce trees. Trees 15(1):50–57
Zweifel R, Zimmermann L, Newbery DM (2005) Modeling tree water deficit from microclimate: an approach to quantifying drought stress. Tree Physiol 25(2):147–156